## Journal of Materials Chemistry B



**PAPER** 

View Article Online



Cite this: J. Mater. Chem. B, 2022, **10**, 10042

# nanoparticles with catechol-grafted poly(ethylene alvcol)†

Increasing the antioxidant capacity of ceria

Yue Hu, Qingbo Zhang, Daniel Garcia-Rojas, Vivian Ling, Caitlin M. Masterson, Yidan Bi, Zhen Xiao, Xiaoting Guo, Jake Villanova, Joshua Dunn and Vicki L. Colvin 🕩

Ceria nanoparticles are remarkable antioxidants due to their large cerium(III) content and the possibility of recovering cerium(III) from cerium(III) after reaction. Here we increase the cerium(III) content of colloidally stable nanoparticles (e.g., nanocrystals) using a reactive polymeric surface coating. Catecholgrafted poly(ethylene glycols) (PEG) polymers of varying lengths and architectures yield materials that are non-aggregating in a variety of aqueous media. Cerium(iv) on the ceria surface both binds and oxidizes the catechol functionality, generating a dark-red colour emblematic of surface-oxidized catechols with a concomitant increase in cerium(iii) revealed by X-ray photoemission spectroscopy (XPS). The extent of ceria reduction depends sensitively on the architecture of the coating polymer; small and compact polymer chains pack with high density at the nanoparticle surface yielding the most cerium(III). Nanoparticles with increased surface reduction, quantified by the intensity of their optical absorption and thermogravimetric measures of polymer grafting densities, were more potent antioxidants as measured by a standard TEAC antioxidant assay. For the same core composition nanoparticle antioxidant capacities could be increased over an order of magnitude by tailoring the length and architecture of the reactive surface coatings.

Received 8th April 2022, Accepted 20th June 2022

DOI: 10.1039/d2tb00779g

rsc.li/materials-b

#### Introduction

By virtue of their large surface area and crystalline structure, nanoparticles can participate in reactions that have no direct molecular analog. 1 Ceria nanoparticles, for example, can both absorb and release oxygen giving rise to both pro- and antioxidant behaviour in water depending on the conditions. Such flexible reactivity relies on the coexistence of both Ce(III), an oxygen-absorbing reductant, and Ce(IV), an oxidant, at the nanoparticle surface. Essential for the between Ce(III) and Ce(IV) in nanoparticles is the stabilization of oxygen vacancies at the particle surface leading to more Ce(III) in nanoparticles as compared to bulk CeO2.2,3 As a result ceria nanoparticles, sometimes referred to as nanozymes, behave as antioxidants able to neutralize many types of biologically relevant reactive oxygen species (ROS).4 While cerium(III) can be oxidized to cerium(iv) quite efficiently in water, over days and weeks fully oxidized nanoparticles eventually return their more reduced state with renewed cerium(III).<sup>5-7</sup> Such perpetual antioxidants have many interesting applications especially in medicine

 $Department\ of\ Chemistry,\ Brown\ University,\ USA.\ E-mail:\ vicki\_colvin@brown.edu$ † Electronic supplementary information (ESI) available. See DOI: https://doi.org/ 10.1039/d2tb007799

where they can act as anti-inflammatory agents, as well as therapeutics for retinal disease and neurodegeneration.8-12

Increasing the antioxidant performance of nanoparticle ceria requires schemes that tilt the balance of cerium redox states towards the more reduced cerium(III) character. 13 To date, materials strategies for achieving this goal have primarily leveraged dimension control, 14 but factors such as particle purity, 15 shape, 16 and polymer architecture can also influence antioxidant performance.<sup>5</sup> As ceria nanoparticles become smaller, oxygen vacancy formation is promoted increasing the content of Ce(III) with the expected increases in antioxidant capacity.14 There are limits, though, to this approach as even in the smallest nanoparticles only 30 to 40% of the total cerium is in a reduced form. 3,17 Antioxidant performance can also be affected by the accessibility of Ce(III) on nanoparticle surfaces. In biological settings surface coatings are necessary for nanoparticle stability, but they can also present a barrier to ROS reaching the reactive particle surface.4 Bulky, grafted polymers that are not well packed at the interface can offer a compromise between colloidal stability and antioxidant reactivity. 18 While there have been a wide variety of polymeric coatings applied to ceria nanoparticles, none have been used to shift the balance between the reduced and oxidized forms of cerium towards the antioxidant Ce(III) state. 4,5

Existing work suggests that with the appropriate design, particle surface coatings could be tailored to enhance the antioxidant capacity of this important class of materials. Small molecules easily oxidized in water, such as catechol and its derivatives, can bind to iron oxide materials, for example, leading to towards an increase in more reduced Fe(11). 19-21 Interestingly the oxidized molecules remained bound to the nanoparticles.<sup>22</sup> Similar chemistry has also been observed in ceria nanoparticles which can both oxidize and bind small molecules including various catechol derivatives. 4 This reaction is characterized by notable colour changes as the colourless molecules turn a dark, typically brownish red once associated with the nanoparticle interface.<sup>23</sup> Toxicologists studying the effects of nanoscale ceria in biological systems have noted the relevance of this oxidation chemistry to the transformations of biomolecules such as dopamine.24 Additionally the colorimetric changes observed as ceria oxidizes small molecules can be exploited in paper-based antioxidant assays.<sup>25</sup> As expected from the reduction-oxidation chemistry, the oxidation of catechol molecules by ceria nanoparticles does yield Ce(III) as a by-product.<sup>26</sup> While catechol-treated ceria nanoparticles are not colloidally stable in water, the solid phase product does have greater reactivity towards superoxide anions.<sup>23</sup>

Here we exploit the oxidative reactivity of ceria nanoparticles towards catechols to increase cerium(III) content and by extension the nanoparticles' antioxidant capacity. The colloidal stability of the materials is preserved by using catecholterminated polymers as surface coatings for nanoparticle ceria. We first synthesize catechol-functionalized polyethylene glycol (PEG) and use it to coat uniform and crystalline ceria nanoparticles ( $d = 5.1 \text{ nm} \pm 1.0 \text{ nm}$ ) prepared in organic media.<sup>27</sup> The catechol coordinates to the surface cerium atoms increasing the cerium(III) content and causing a distinct colour change representative of surface-oxidized catechols. These materials outperform ceria nanoparticles stabilized by PEG polymers bound to the surface with less reactive species. The impact of catechol-polymers on the nanoparticle antioxidant properties and cerium(III) content depends sensitively on the grafting density of the coating. As the chain length of linear catechol-PEG increases from 2000 to 30000, fewer polymer chains are bound per particle and ultimately this results in lower antioxidant capacities as there is less surface reduction. Similarly, branched catechol-PEG packs poorly at the particle interface leading to faster antioxidant reactivity in standard assays but less overall antioxidant capacity. This trend is the opposite observed for non-reactive surface coatings in which lower grafting densities optimize both the capacity and speed of Ce(III) reduction reactions. 4,5 For reactive surface coatings such as the catechol-PEG systems, short and compact structures lead to more grafting density and more antioxidant capacity.

#### Results and discussion

Ceria nanoparticles can be formed via the high-temperature thermolysis of cerium(III) salts solubilized by amines in organic media.<sup>28</sup> In this reaction, cerium nitrate transforms to a stable, light yellow amine complex in octadecene at modest temperatures of 80 °C under an inert atmosphere (Scheme S1, ESI†). Further heating to 240 °C leads to the thermal decomposition of the organic amines and the generation of ceria nanoparticles. The resulting solutions after nanoparticle formation are a dark brown colour and are more intensely coloured for larger sizes. By increasing the amount of organic amine relative to the cerium nitrate, it is possible to tune the diameters of the nanoparticles from 4 to 13 nm.<sup>28</sup> This synthetic strategy generates relatively monodisperse nanoparticles with dimensional dispersity generally under 20% and products that are highly crystalline with a monoclinic structure (Fig. 1).

Bulk ceria is a face-centered cubic crystal and crystalline nanoparticle ceria adopts a similar structure. 29 As expected, the peak position of the (111) reflection is broadened in the smallest particles (Fig. S1, ESI†) as expected for the smallest crystallites. Notably, the peak also shifts to smaller two-theta or larger d-spacings with decreasing particle dimension. This phenomenon has been associated with an increasing amount of oxygen vacancies and greater cerium(III) content in the nanoparticle (Table S1, ESI†).14 The fact that the shift is more pronounced in smaller crystallites is attributed to the fact that cerium(III) content increases with decreasing size.<sup>30</sup>

The organic amine used in the reaction, here oleylamine, both coats the surface of the nanoparticle ceria and exists as a free molecule in the homogeneous nanoparticle suspensions. Product solutions in hexanes typically contain 8000 ppm of cerium atoms or 40 micromolar cerium (e.g., one 4.5 nm diameter nanoceria contains ~1000 cerium atoms) in the case of the smallest nanoparticles. Before purification the native surface coating is present at high concentrations in solution. The integrated infrared absorbance of the C-H stretch region (Fig. S3, ESI†) reveals that before purification particle solutions can contain as much as 290 millimolar of organic amine of which only a small amount is bound to the surface. Oleylamine packed onto a gold surface was found to have an effective occupied surface area of 14 Å<sup>2</sup>. From this we can estimate that a single ceria nanoparticle of 4.5 nm diameter would be coated by several hundred oleylamine molecules contributing micromolar levels of oleylamine (Table S2, ESI†). Samples can be purified, and the free amine reduced, through repeated centrifugation and redispersion cycles after which the particles are easily dispersed in organic media with their native surface coating intact. Further purification can result in irreversible aggregation of the nanoparticles as the native oleylamine coating is removed by prolonged washing. Fig. S2 (ESI†) shows the infrared (IR) spectrum of the solid product recovered from centrifugation of the nanoceria suspensions. After repeated washes, the organic amine features diminish in intensity substantially. Monitoring the IR absorbance is an important tool for optimizing the purification process such that sample solutions have minimal free amines without loss of surfacebound amines.

These hydrophobic oleylamine-coated nanoparticles can be phase transferred into water using polyethylene glycol (PEG).

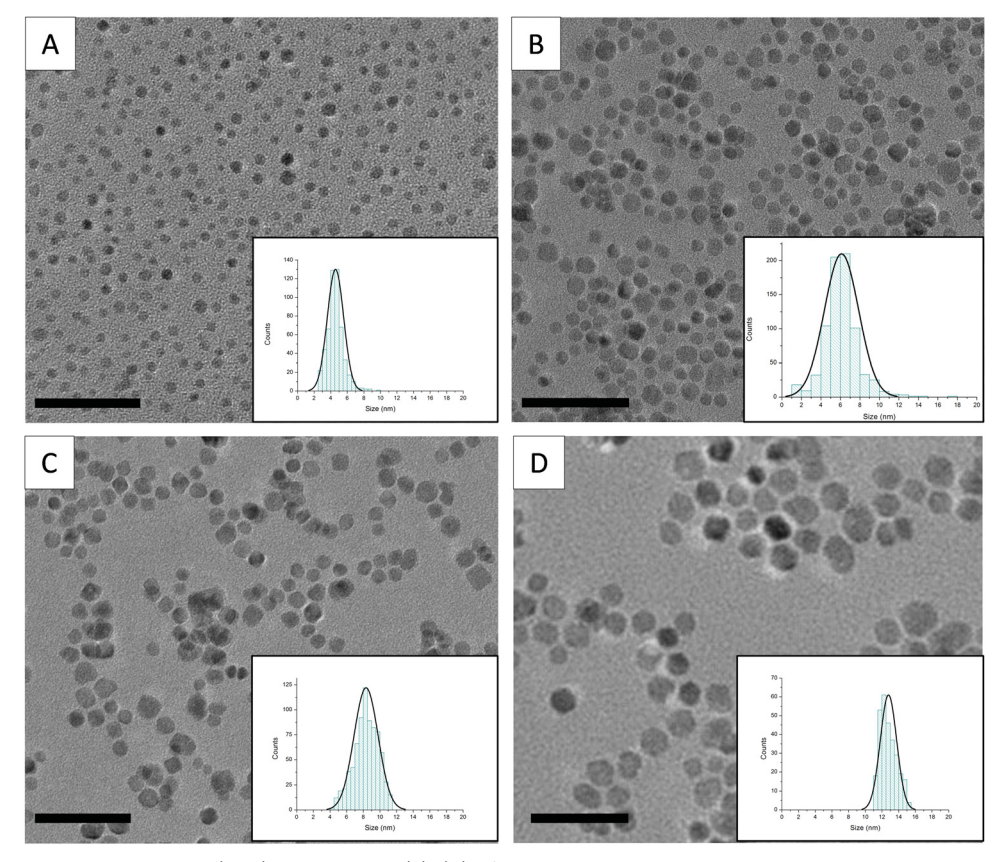


Fig. 1 Transmission electron microscopy (TEM) micrographs. (A)-(D) of oleylamine-coated ceria nanoparticles with diameters: (A) 4.5  $\pm$  0.7 nm; (B)  $6.5 \pm 0.9$  nm; (C)  $8.5 \pm 1.3$  nm; (D)  $12.9 \pm 1.3$  nm. Histograms of the particle diameter distributions area also shown. Scale bars are 20 nm.

PEG is a biocompatible polymer widely applied to nanoparticle coatings.32,33 It is available commercially in many different molecular weights and structures (e.g., linear, branched) and for this work was prepared with free acid end groups that could be coupled to nitrodopamine through the formation of an amide bond.<sup>27</sup> Nitrodopamine is used here instead of dopamine because it is more resistant to oxidation under ambient conditions. COMU (e.g., 1-Cyano-2-ethoxy-2-oxoethylidenaminooxy dimethylaminomorpholino carbenium hexafluorophosphate) is an effective catalyst for promoting this facile coupling chemistry.<sup>34</sup> The catechol-terminated polymers were purified by dialysis after which time they could be dissolved in deuterated solvents for proton NMR analysis.

Proton NMR reveals peaks consistent with successful formation of the nitrodopamine-terminated PEG polymers (Fig. 2(B) and Fig. S4–S8, ESI†) with yields up to 68% (Table S3, ESI†). The proton features at low-field shifts, between 2 to 5 ppm, correspond to the polyether backbone protons as well as those near the amide bond. The peaks occurring far downfield can be assigned to the nitrodopamine terminus. The ratio of the two peaks allows for a semi-quantitative assessment of reaction yield. Briefly, the proton ratio for the aliphatic peaks versus the dopamine peaks can be calculated stoichiometrically and compared to the measured proton NMR results. In the case of the shortest PEG used, 2000 molecular weight, 172 protons are associated with the polyether backbone and give rise to the

signal shown in the green dotted box. Conversely, only two protons indicated by the blue dotted box are bound to the phenyl constituent. All samples had more polymer proton signal than would be predicted if the reaction had 100% yield (Table S3, ESI†); these data permit a reaction yield to be estimated by dividing the integrated ratio of polymer protons by that expected for a pure dopamine-PEG. This approach only provides an estimate as the intensity of proton spin signals at very different chemical shifts is not linearly dependent on proton concentration; however, the approach has been used frequently in the polymer chemistry literature to estimate the success of backbone and termini modification.<sup>35</sup> With that caveat, these data suggest that the yield for the modification of PEG polymers by dopamine is on the order of 50% (Table S3, ESI†).

Scheme 1 outlines the phase transfer methodology used to modify the surface of nanoparticle ceria and form stable aqueous suspensions of particles. Oleylamine-coated particles are sedimented and resuspended in chloroform forming a clear, brown solution (Scheme 1(A)). Typically chloroform solution concentrations are ~2000 ppm cerium (14.3 micromolar in atomic cerium) and catechol-PEG polymers are added to the same solution (Scheme 1(B)). Here a variety of different architectures for the PEG are examined and their structures are shown in Fig. 3(A). The nanoparticle and polymer solution is then mixed using a magnetic stirrer for 20 minutes followed by

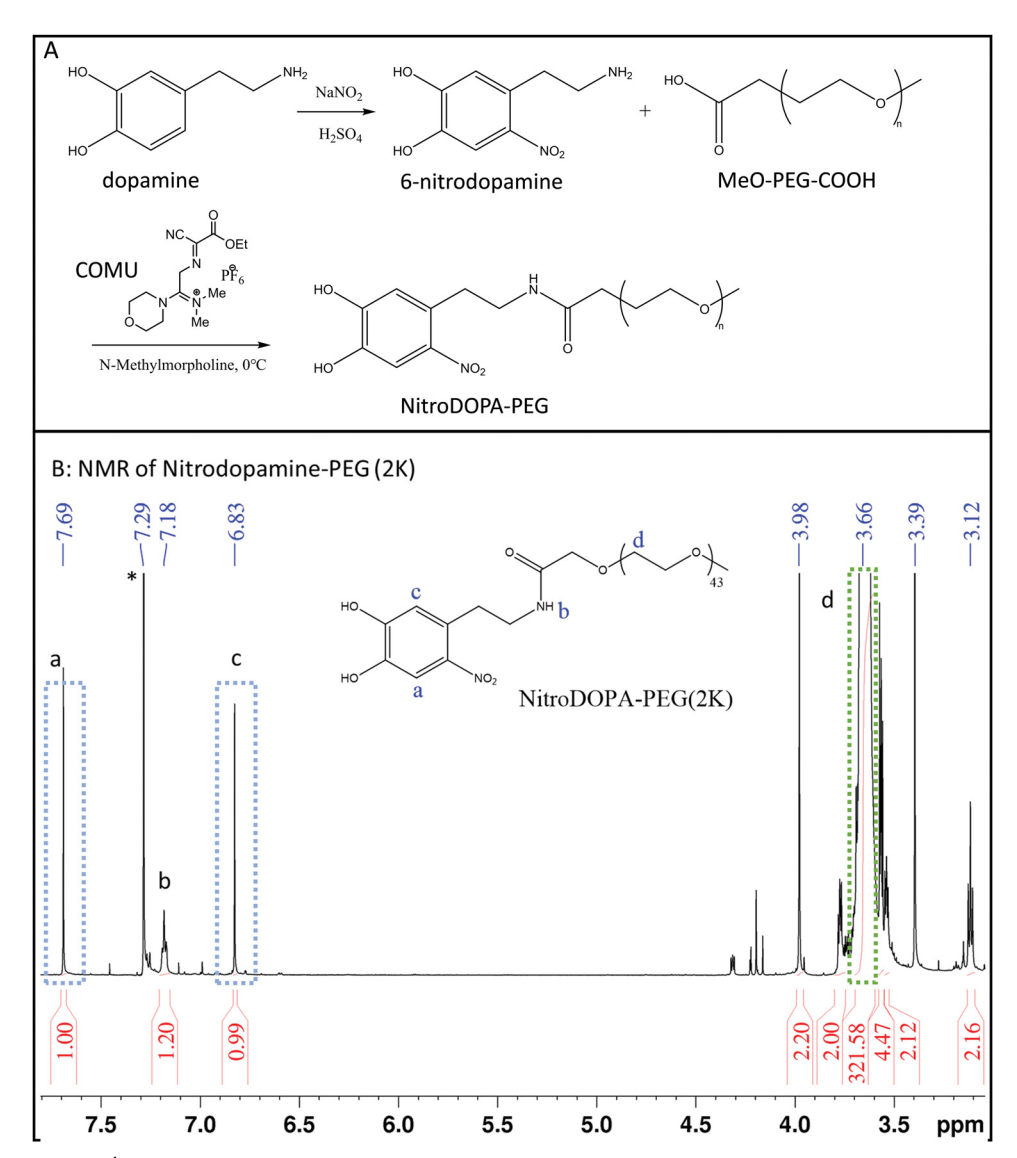


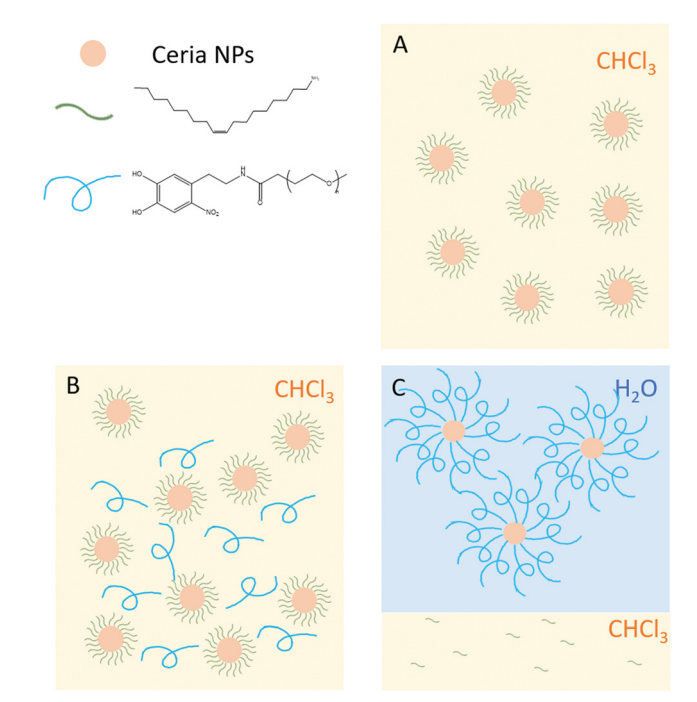
Fig. 2 Synthetic pathway and <sup>1</sup>H-NMR of nitro-dopamine-PEG. (A) Synthetic pathway for the synthesis of nitrodopamine and the coupling to get the nitrodopamine-PEG. (B) The <sup>1</sup>H-NMR spectrum of nitroDOPA-PEG (2K) in CDCl<sub>3</sub>. Red numbers at the bottom are peak areas integrated by Bruker Topspin. The ratio: area of peak (d)/area of peak (a) can be used to estimate the yield of nitroDOPA-PEG. Peak labelled with the star (\*) suggests CDCl<sub>3</sub> solvent residual peak.

the addition of water. Over 12 to 14 hours the chloroform evaporates, leaving behind a clear, brown-yellow solution of ceria Nanoparticles in water. Further purification using syringe filtering and filter centrifugation ensures that free oleylamine and any residual chloroform are fully removed.

Ceria nanoparticle solutions formed in this manner are clear with colours ranging from pale yellow to dark yellow; typical concentrations are 500 ppm in cerium (or 3.6 micromolar in atomic cerium) solution with respect to nanoparticle concentration. Dynamic light scattering (DLS) reveals that the hydrodynamic diameter  $(D_H)$  of the PEG-coated ceria ranges from 20 to 65 nm in water depending on the chain length and structure of the PEG. The polymer coating is a significant contributor to the overall dimensions of the material in solution and after coating a 4.5 nm diameter nanoparticle with PEG the

hydrodynamic diameter, including the polymer, is 24.8 nm.<sup>36</sup> The materials are stable in phosphate-buffered saline (PBS) with identical hydrodynamic diameters and no visible aggregation (Fig. 4(B)). Cryogenic transmission electron microscopy of the solutions shows nanoparticles that are well dispersed with no evidence of aggregation in agreement with the light scattering results (Fig. 4(C) and (D)). Particles are amenable to freezedrying and can be resuspended in water after prolonged storage from this dried form (Fig. S9B, ESI†).

The nature of the polymer coating, both its length and its structure, has a notable effect on the ceria-polymer hydrodynamic diameter as well as the number of polymer chains bound to each nanoparticle. For the linear PEG polymer coatings, the hydrodynamic diameter of the material increases with increasing molecular weight (Fig. 4(B)). For example, nanoparticles



Scheme 1 Organic-aqueous phase transfer for forming stable aqueous suspensions of ceria nanoparticles. (A) Dispersion of oleylamine-coated ceria NPs in CHCl3. (B) NitroDOPA-PEG and ceria NPs in CHCl3. (C) The cholorform/water solution is stirred at room temperature as the chloroform evaporates leaving nitroDOPA-PEG-coated ceria NPs in water.

coated with 2000 MW PEG have a  $D_{\rm H}$  of 24.8 nm, while those coated with 30 000 MW PEG have a  $D_{\rm H}$  of 67.2 nm. While longer polymers do increase the hydrodynamic diameter, the effect is not easily predicted solely based on chain length. This is

because polymer chains bound to nanoparticle surfaces undergo a rod-to-coil transition as a function of chain length. As a result, the longer polymer chains form a mushroom structure leading to smaller hydrodynamic diameters than that predicted if they were extended completely.<sup>37</sup> Interestingly, the branched PEG gives rise to more compact structures than their linear counterparts; the average  $D_{\rm H}$  of 5000 MW linear PEG-coated ceria is 22.6 nm while that of larger branched PEG ceria is nearly 90 nm (Fig. 4(B)). The number of polymers bound to a ceria nanoparticle is dependent on the conformation and chain length of the PEG coating material.<sup>38</sup> For a process that utilizes a 'grafting-to' method for coating nanoparticles with polymers, the density of surface coating materials is limited by the polymer's physical dimensions and the steric interactions between adjacent chains. 18 Polymers that adopt a coil conformation, typically larger molecular weight or branched materials, will provide the lowest grafting densities. Conversely, compact polymers will pack tightly and coat nanoparticles at a greater density. 18,39 Thermogravimetric analysis (TGA) was applied to ceria-polymer solid samples to evaluate the grafting density of the materials (Fig. S10, ESI†). Complete combustion of all carbon content results from this process allowing for the number of polymer chains at the particle interface, or the grafting density, to be calculated. 40 Fig. 3(B) shows that as the molecular weights of both the linear and branched polyethylene glycol increase, there is a decrease in the grafting density and the number of chains bound per particle (see also Table S4, ESI†). The lower molecular weight polymers have on the order of six times more polymer chains bound than the larger polymer coatings, a finding in good agreement with other studies of grafting-to nanoparticle-polymer systems.<sup>18</sup>

The oxidation of a catechol, here derived from nitrodopamine, at the particle interface is expected to yield increased cerium(III)

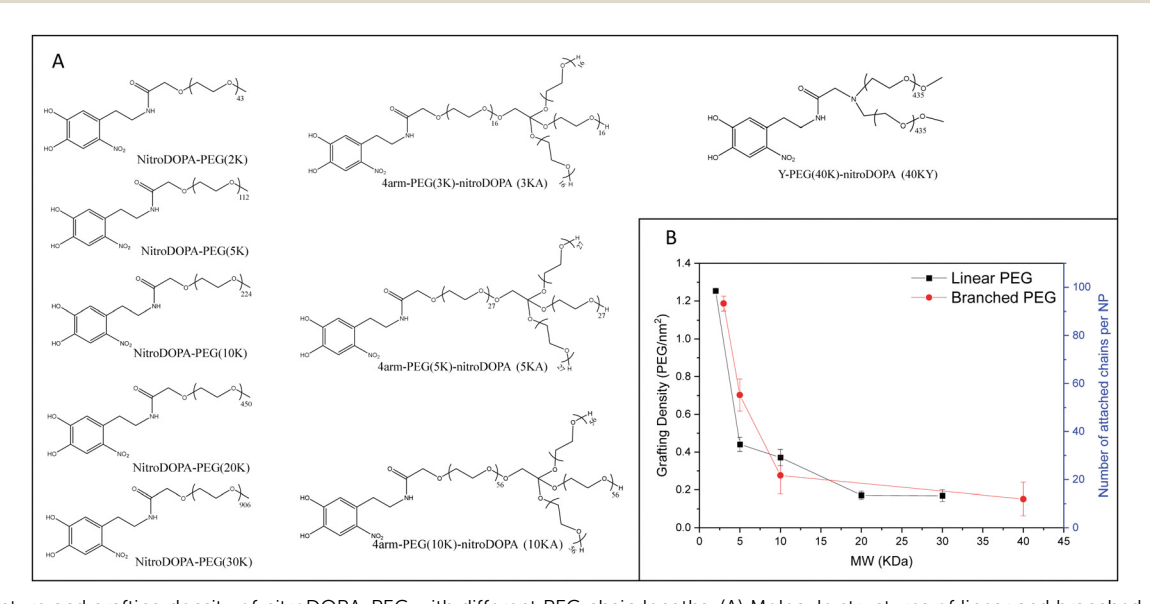


Fig. 3 Structure and grafting density of nitroDOPA-PEG with different PEG chain lengths. (A) Molecule structures of linear and branched nitroDOPA-PEG polymers. (B) Grafting densities of linear(black) and branched(red) nitroDOPA-PEG-coated nanoparticles decrease while PEG chain lengths increase. Thermogravimetric analysis (TGA) was collected on the Mettler Toledo TG50 Thermogravimetric with an analyzer using an alumina crucible. All samples started with a mass at 3-5 mg. Samples were first heated to 90 °C and held for half an hour to get rid of the humidity. The heating rate of the analysis was 20 °C min<sup>-1</sup> between 100 and 950 °C, under air atmosphere with a flow rate of 80 mL min<sup>-1</sup>. All samples were tested three times.

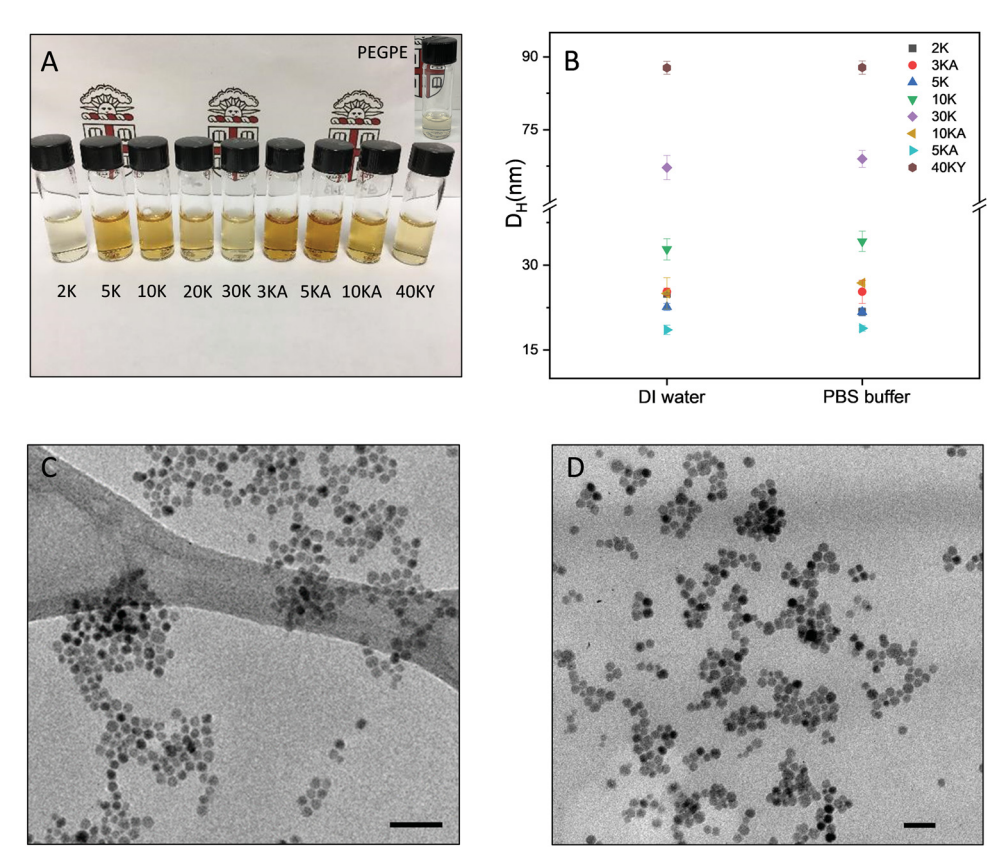
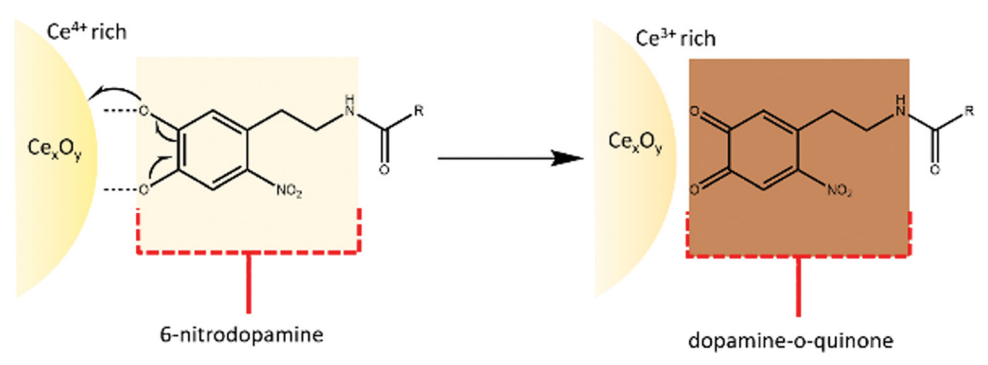


Fig. 4 Ceria nanoparticles in aqueous solution. (A) Ceria nanoparticles (4.5  $\pm$  0.7 nm) in aqueous solutions at 500 ppm (5K, 10K, 20K, 3KA, 5KA, 10KA, 40KY, PEGPE), and 100 ppm (2K). The solution contains more nitroDOPA-PEG presents a darker colour. (B) The mean and relative variance of the size distributions of the ceria nanoparticles were measured by DLS in water and PBS buffer. Cryo-TEM photo of the NitroDOPA-PEG-coated ceria nanoparticles: (C) nitroDOPA-PEG (2K) coated, and (D) 4arm NitroDOPA-PEG (10K) coated. Scale bars are 20 nm.

content (Scheme 2). The oxidation of catechols to quinones in water is often associated with the reduction of the metal centers to which they are bound. 41,42 Such chemistry has been observed on both iron oxide nanoparticles and ceria nanoparticles.<sup>4,21</sup> The Ce(IV)/Ce(III) couple in water is 1.74 V while Fe(III)/Fe(II) is 0.77 V suggesting thermodynamically such a redox reaction is possible. 43,44 Ceria nanoparticles can also oxidize polyphenol compounds, such as ascorbic acid, gallic acid, caffeic acid, and dopamine.23,26

The result of this reaction is the formation of oxidized products, quinones or semiquinones, along with reduced metal centers. 45 Scheme 2 illustrates this chemistry in the case of the ceria nanoparticles, where the initially pale-coloured fully oxidized ceria is converted to a brown-red material containing substantial amounts of cerium(III). 25,26,46 Quinones oxidized from L-dopamine have increasing strong optical absorption features that can be measured in these materials. 47 Andreescu et al. noted that the colour change is due to the change of



Scheme 2 Nitro-DOPA functional group was oxidized to dopamine-o-quinone structure by Ce<sup>4+</sup> on the surface of nanocrystal. This redox process generates a strong binding between ceria and nitroDOPA-PEG polymer, meanwhile Ce3+ content on the surface of nanocrystal increases during the redox reaction, which improves the antioxidant capacity of ceria nanoparticles. Modified from Hayat et al. 2014.

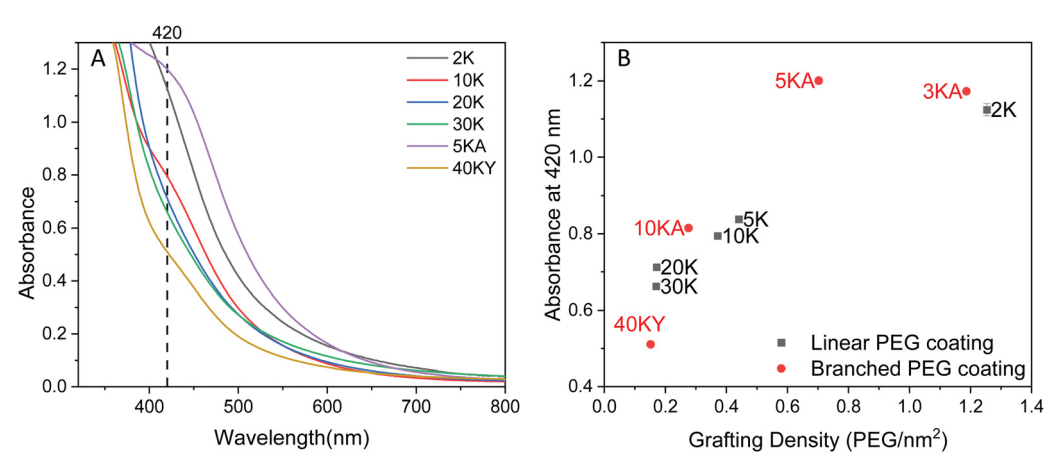


Fig. 5 UV absorbance of nitroDOPA-PEG grafted ceria nanoparticles. (A) Absorbance spectra of ceria nanoparticles with different nitroDOPA-PEG coatings at a cerium concentration of 500 ppm (5K, 20K, 30K, 5KA, 40KY), and 100 ppm (2K). (B) UV-vis absorbance at 420 nm of ceria nanoparticles with different NitroDOPA-PEG coatings is positively related to nitroDOPA grafting density on the surface of nanoparticles. The absorbance of the 2K coated sample was multiplied by five to account for the different nanocrystal concentration.

oxidation state and formation of the surface complexes of dopamine-o-quinone with the ceria nanoparticles. 48 Ceria nanoparticles when mixed with benzoquinone had notable colour changes that could be tracked *via* absorbance. <sup>26</sup> Sharpe et al. quantified that the colour change is linear with catechol concentration allowing for design of a nanoceria-based antioxidant assay based on this property.23 The colour change of these samples thus provides one measure of the extent of catechol modification of the nanoparticle surface. Fig. 5(A) shows the optical absorption spectra of the various catechol-PEG coated ceria nanoparticles. While the spectra are relatively featureless, the absorbance at 420 nm is a convenient measure of the oxidative surface chemistry. Samples coated with the smallest polymer chains exhibit the most notable visible colour both in solid form (Fig. S9B, ESI†) and when dissolved in water (Fig. 4(A)). Fig. 5(B) compares the absorbance after surface modification with the grafting density of the polymer-nanoparticle samples; each polymer is terminated by a catechol. In general, samples that have higher grafting densities of polymer have more oxidized catechol. This suggests that cerium(III) content increases in these samples because of the oxidized quinone consistent with the expectations in Scheme 2.

X-ray photoemission spectroscopy (XPS) (Fig. S13–S18, ESI†) supports these data by providing an estimate of the Ce(III) content and, indirectly, level of oxygen vacancies in these materials, and finds an increase in Ce(III) content that correlates well with the grafting density of the reactive polymers. These data should be viewed cautiously as photochemistry can be initiated by X-ray irradiation of ceria nanoparticles under vacuum making quantification of cerium(III) content by XPS problematic. 49,50 Still the extent of this process is likely independent of surface coating, and we note that the qualitative trends observed are consistent with Fig. 5 as samples with more oxidized catechol content also had greater cerium(III) content (Fig. S19, ESI†).

To evaluate these materials as antioxidants, we performed specific chemical experiments to evaluate the ability of the various ceria samples to block oxidation reactions. Trolox (6-hydroxy-2,5,7,8-tetramethylchroman-2-carboxylic acid) equivalent antioxidant capacity (TEAC) assay using sodium fluorescein (FL) as the probe are a common method to assess the antioxidant capacities of ceria nanoparticles in the aqueous environment (Fig. 6). We also examined other antioxidant probe assays with similar findings (Fig. S12, ESI†). The decay of the probe intensity triggered by thermolysis of a radical generator (AAPH) was tracked by a microplate reader under 37 °C with the protection of different nanoparticles. Ceria nanoparticles with more robust antioxidant capacity result in a slower probe decay, and the area under the curve (AUC) can be used as a measure of this protection.

Fig. 6(D) and Table 1 show the strong correlation between the polymer grafting density of the nanoparticles and their antioxidant capacity. For the reactive coatings of interest here, the best materials result from short and compact polymers that pack tightly at the interface. Notably a phospholipid-PEG coating (PEGPE) without any catechol content was the least reactive ceria formulation examined. As we compare the linear catechol-PEG coatings, ranging from 2000 to 30 000 molecular weight, we see a clear increase in the antioxidant capacity with the maximum reactivity occurring for particles coated with the lower MW polymers. As is clear in Fig. 5(B) this trend reflects the increasing oxidized catechol content of the shorter chain coatings made possible from their more compact packing. Similarly, the branched catechol-PEG coating also yield ceria materials with stronger antioxidant properties when the polymer grafting densities are higher. The one exception, the three-arm branched (3KA), is notable as it's the one sample for which higher grafting densities did not translate into more oxidized catechol content as measured by optical absorption (Fig. 5(B)).

The data also reveals that the branched catechol–PEG polymers outperformed the linear catechol-polymers. For non-reactive polymer coatings others have noted the advantage of bulky polymers in facilitating surface access of oxidants.<sup>4,5</sup> While this effect would more likely play a role on the kinetics

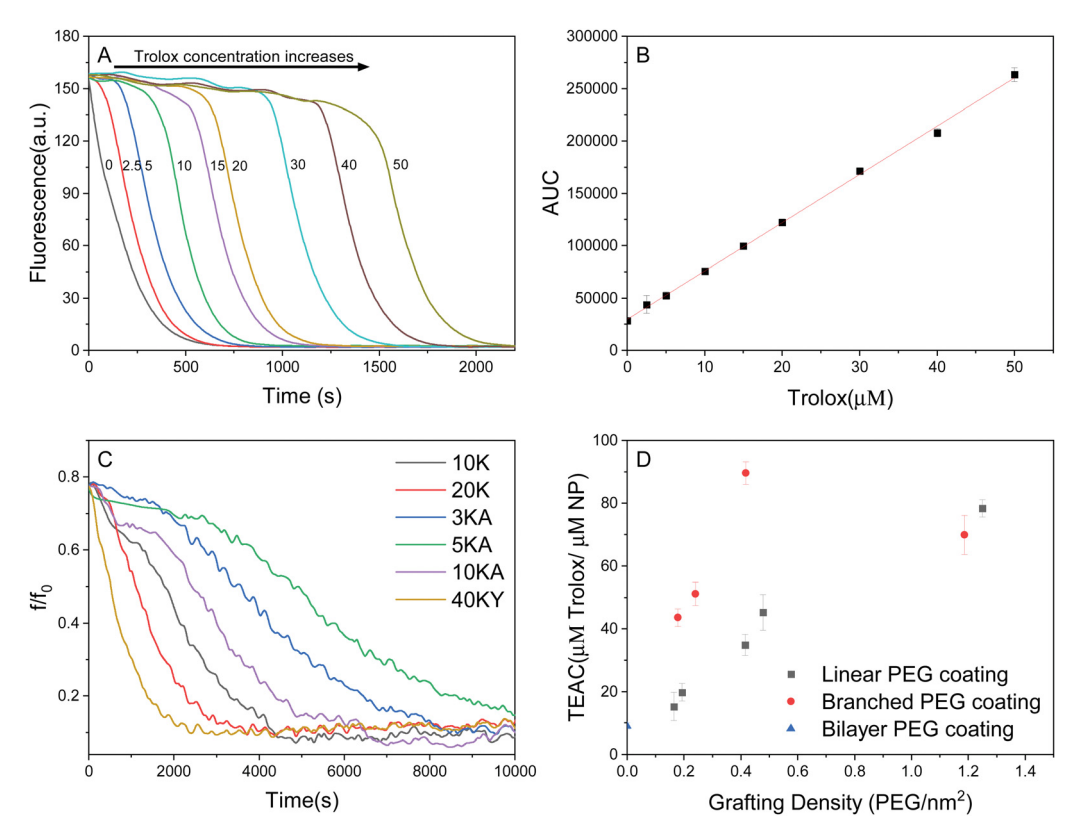


Fig. 6 Evaluation of antioxidant capacity for ceria nanoparticles by Trolox (6-hydroxy-2,5,7,8-tetramethylchroman-2-carboxylic acid) equivalent antioxidant capacity (TEAC) assay using sodium fluorescein (FL) as the fluorescent probe. (A) FL decay caused by radicals generation from AAPH thermolysis under 37 °C. Numbers in the panel show the Trolox added in µM. (B) The final antioxidant capacity values were calculated using a regression equation between the Trolox concentration and the net area under the FL decay curve (AUC). (C) FL fluorescence decay curves corrected by deducting probe-nanocrystal interaction induced by AAPH thermolysis in the presence of ceria nanoparticles (200 ppm) with different surface coatings. (D) Trolox equivalent antioxidant capacity (TEAC) values of ceria nanoparticles with different PEG coatings compared to their grafting densities.

Table 1 Antioxidant capacities of nitroDOPA-PEG-coated ceria nanoparticles measured from TEAC-fluorescein assay compared to ceria-based material in other works. TEAC is expressed as µmol Trolox per gram of cerium oxide

Literature	Samples	TEAC (μmol TE g <sup>-1</sup>
This work	2K	316
	5K	158
	10K	128
	20K	67
	30K	40
	3KA	259
	5KA	358
	10KA	196
	40KY	168
	PEGPE	32
Lee 2013 <sup>5</sup>	CeO <sub>2</sub> @OA	24
	CeO <sub>2</sub> @PMAO	4
Marino 2017 <sup>51</sup>	Gelatin/nanoceria nanocomposite fibers	110
Tian 2017 <sup>52</sup>	Porous nanorods of ceria	44
	Nonporous nanorods of ceria	13
	Aggregated nanoceria	7

of the oxidation process, as opposed to the overall antioxidant capacity, these could be confounded to some extent in the TEAC assay. Finally, we compared the performance of these materials to those reported for other types of ceria nanostructures (Table 1).<sup>5,51,52</sup> It is convention to report the TEAC capacities against the net mass of cerium oxide, not available surface area, as this is an experimentally well-defined parameter. The materials reported here do show greater antioxidant capacities than nanoscale ceria produced in a similar process as well as by nanoscale ceria made through aqueous syntheses.5,51,52

#### Conclusions

The reaction between catechol-PEG and ceria nanoparticles provides for colloidally stable nanoparticles in water with high antioxidant capacities. In these materials the surface oxidation of a catechol derivative by cerium(iv) yields as a by-product increased cerium(III) content and as a result more capacity for antioxidant behaviour. By using short and compact reactive coatings with high grafting densities, we see a tenfold increase in antioxidant capacity for the same core ceria nanoparticle. Additionally, a method to stabilize nanoscale ceria in a more reduced state will also limit its oxidative reactivity, which may reduce its propensity to oxidize important extracellular biomolecules.

### Experimental

#### Synthetic procedures, materials and methods

Rhodamine B (RhB, ≥ 96%), fluorescein sodium salt (fluorescein),  $(\pm)$ -6-hydroxy-2,5,7,8-tetramethylchromane-2-carboxylic acid (Trolox, 97%), 2,2'-azobis(2-methylpropionamidine)dihydrochloride (AAPH, granular, 97%), phosphate buffered saline (PBS, 10×), cerium (III) nitrate hexahydrate(Ce(NO<sub>3</sub>)<sub>3</sub>·6H<sub>2</sub>O, 99%), sodium nitrate (NaNO<sub>3</sub>, ≥99%), oleylamine (70%), 1-octadecene (90%), oleic acid (≥ 99%), dopamine hydrochloride, (1-Cyano-2ethoxy-2-oxo ethylidenaminooxy) dimethylamino-morpholinocarbenium hexafluorophosphate (COMU, 97%), 4-methylmorpholine ( $\geq$ 99%) were purchased from Sigma Chemical Co. (St. Louis, MO, USA). Poly(ethylene glycol) methyl ether thiol (mPEG-SH, MW 10K) was purchased from Creative PEGWorks (NC, USA). 4arm PEG, 3arm-Hydroxyl, 1arm-Acetic Acid (MeO-PEG-COOH, MW 3K, 5K, and 10K), and Y-PEG(40K)-NHS were purchased from JenKem Technology USA. 1,2-Dioleoyl-sn-glycero-3-phosphoethanolamine-N-[methoxy(polyethylene glycol)-2000] (ammonium salt) (18:1 PEG2000-PE, > 99%) was purchased from Avanti Polar Lipids (USA). Deionized (DI) water with a resistivity of 18.2 M $\Omega$  cm was used in all experiments.

All solutions are prepared just before the experiment. Stock solutions of pyranine (500  $\mu M)$ , rhodamine B (500  $\mu M)$ , sodium fluorescein (400  $\mu M)$ , Trolox (1500  $\mu M)$  are prepared with phosphate buffer (1×) and dilute to the concentrations of working solutions(5–100  $\mu M)$ . AAPH (10–50 mM) solutions are made respectively by dissolving the powder in PBS buffer. Ceria nanoparticles (0.1–5 nM) were also diluted by phosphate buffer right before the measurement.

#### Synthesis of ceria nanoparticles with a core diameter of 4.5 nm

The ceria nanoparticle synthesis method was modified from Lee et al.<sup>28</sup> Briefly, 1 mmol of Ce(NO<sub>3</sub>)<sub>3</sub>·6H<sub>2</sub>O, 3.0 mmol of oleylamine, and 4.0 g 1-octadecene were mixed in a 50 mL 3-necked flask at 80 °C for 30 min, forming a brownish-yellow mixture. Then the temperature was increased to 120 °C for 30 min to evaporate the low-boiling point impurity. After that, the reaction was heated up to 260 °C for 2 hours. The final product was washed at least five times until the final product is not viscous. One wash means nanoparticles were precipitated with acetone (Sigma, >99.5%) and methanol (Sigma,  $\geq$  99.85%) (volume ratio = 1:1). Then the sediment was collected by centrifugation (9000 rpm, 15 min) and redispersed into hexane (>98.5) or CHCl<sub>3</sub> (Sigma, >99%). The size of nanoparticles 4.5  $\pm$  0.7 nm was determined at 200 kV by a JEOL 2100F high-resolution transmission electron microscopy. Synthesis of nanoparticles with larger core diameters (6.5-12.9 nm) was using the same method while increasing the concentrations of Ce(NO<sub>3</sub>)<sub>3</sub>·6H<sub>2</sub>O (1-10 mmol) and oleylamine (1-30 mmol) in the reaction.

#### Synthesis of NitroDOPA-PEG

This synthesis was modified from Lassenberger *et al.* (2016).<sup>27</sup> One gram of dopamine was first dissolved in 30 mL DI water, and 1.3 g sodium nitrate was added into the solution under

vigorously stirring in an ice bath. Then 10 mL sulfuric acid (20% v/v) was added to the solution dropwise. The ice bath was removed, and the mixture was stirred at room temperature for at least 12 hours. Nitrodopamine hydrogensulfate (DOPA) was obtained by filtering the final product and washed with cold DI water several times. Then DOPA was freeze-dried into a powder and stored in the refrigerator. To get DOPA-PEG, 0.5 mmol MeO-PEG-COOH (4arm PEG, 3arm-Hydroxyl, 1arm-Acetic Acid, MW 10 kDa) was dissolved in 10 mL DMF at 37 °C and cooled to 4 °C under an ice bath. COMU ((1-Cyano-2-ethoxy 2-oxoethylidenaminooxy) dimethylamino-morpholino-carbenium hexafluorophosphate) 0.6 mmol was dissolved in 2 mL DMF. Then COMU solution and N-methylmorpholine (6 mmol) were added into the mixture, and the mixture was kept at 4 °C and stirred for 20 minutes. A nitrodopamine (0.6 mmol) solution in 2 mL DMF was added to the mix dropwise. The reaction was stirred at 4 °C for 2 hours then at room temperature for 16 hours. The product was dialyzed in DI water for 48 hours and collected by freeze-drying (Fig. S9A, ESI†). 1H-NMR spectra were obtained by Bruker high field NMR 600 (MHz) in CDCl<sub>3</sub> (99.5%, Cambridge Isotope Laboratories).

#### Phase transfer of ceria nanoparticles

About 10–20 mg nitroDOPA-PEG was dissolved in 1 mL chloroform. Ceria nanoparticles were pre-suspended in chloroform (10 mg mL<sup>-1</sup>). 1 mL nitroDOPA-PEG solution and 1 mL ceria colloidal solution were mixed at room temperature for 20 min. Then 3 mL DI water was added to the system. The mixture was kept stirred for over 24 hours to let the chloroform entirely evaporated. The final product was purified with a 0.2-micron syringe filter, then washed with DI water three times using a centrifugal filter (100 KDa, Pall) under centrifugation (3000 rpm, 5 minutes). Phase transfer yield can go up to 98%.

#### Antioxidant capacity measurement

The method used was modified from Gregório *et al.* (2010), based on the ORAC assays method described in their paper. The experiments were developed under the 96-well plate with a final concentration of 250  $\mu L$ . For TEAC-pyranine and TEAC-rhodamine B assays, Trolox or nanoparticles solution 100  $\mu L$  were mixed with 20  $\mu L$  pyranine or rhodamine B and 50  $\mu L$  PBS. The mixture solution was incubated at 37 °C for 15 min. Then 80  $\mu L$  AAPH was injected into the mixture placed in each well by using a multichannel pipette. Then the plate was transferred quickly to the plate reader. The UV absorbance signals were collected every 30 seconds for 5 hours at 454 nm (pyranine) or 555 nm (rhodamine B) at 37 °C, with the plate was shaken 3 seconds before each reading. Each experiment was duplicated and repeated at least three times on a different day.

#### ORAC assay using sodium fluorescein as the probe

Samples were assayed following the procedure described in Ou et al. (2001). Trolox (0–100 ppm) or nanoparticles (0.1–5 nM) 25  $\mu$ L were added to wells in a 96 black-welled plate. Then 150  $\mu$ L sodium fluorescein (40 nM) was added to each well, and the plate was incubated for 15 min at 37 °C. A 25  $\mu$ L AAPH

solution (150 mM) was injected into all wells by using a multichannel pipette. The plate was transferred quickly to the plate reader with an excitation filter of 485 nm and an emission filter of 535 nm. The fluorescent signal was read every 30 seconds for 3 hours to reaction completion, with the plate shaken 3 seconds before every reading. All tests were performed in triplicate.

#### Transmission electron microscopy (TEM)

TEM was acquired by the JEOL 2100 Field Emission Gun Transmission Electron Microscope at an acceleration voltage of 200 kV. Five microliters of the ceria nanoparticle solution with a concentration of 500 ppm were dropped on a 200 mesh carbon-coated copper grid (Polysciences, USA). After complete evaporation of the solution, the nanoparticles were deposited on the copper grid and were ready for TEM measurement. The nanoparticles diameters were analyzed by ImageJ. The average diameters and size distribution were determined from the measurement of at least 1000 nanoparticles.

#### Zeta potential and dynamic light scattering (DLS)

All zeta potential and DLS reported in this paper were measured at room temperature on a Zetasizer Nano ZS (Malvern Instruments Ltd, Malvern, UK). Zeta potential was measured in a folded capillary cuvette, and DLS was measured in a disposable 10 mm pathlength cuvette. All samples were measured in triplicate (Fig. S11, ESI†).

#### Thermogravimetry analyzer (TGA)

Mettler Toledo TG50 Thermogravimetric with analyzer using an alumina crucible was used in TGA measurements at a heating rate of 20 °C min<sup>-1</sup> between 25 and 950 °C. The analysis was performed under the air atmosphere with a flow rate of 80 mL min<sup>-1</sup>. All samples were measured in triplicate.

#### X-ray powder diffraction (XRD)

X-ray diffraction pattern for the ceria nanoparticles with different diameters was taken by Bruker D8 Discovery 2D X-ray Diffractometer (Cu K $\alpha$ ,  $\lambda$  = 1.54056 Å). A 0.5 mL nanoparticle solution with a cerium concentration of 1000 ppm was dropped on a glass sample holder. After the solution fully evaporated, a thin layer of nanoparticles remained on the glass slide, and the XRD diffraction pattern was taken from  $10^{\circ}$  to  $90^{\circ}$ . The crystallite grain size was calculated based on the full width at half maximum (FWHM) of the (111) peak centered at 28.75° by using the OriginLab peak analyzer function. It was calculated as the following Scherrer equation:<sup>55</sup>

Grain Size = 
$$\frac{0.94\lambda}{\text{FWHM} \cdot \cos \theta}$$

#### Fourier-transform infrared spectroscopy (FTIR) spectra

FTIR spectra of oleylaime on ceria nanoparticles were obtained by FTIR-6000 Series Spectrometer (Jasco, Europe) with a sealed liquid cell sample holder with CaF<sub>2</sub> window; pathlength = 0.1 mm (Jasco, Europe). Ceria nanoparticles were dispersed in

CCl<sub>4</sub> and injected into the liquid cell. The cell was then inserted into the equipment, and FTIR spectra were recorded in the region of 4000-400 cm<sup>-1</sup> at room temperature. All samples were measured in triplicates, and the C-H stretch peak was found and integrated by Spectra Manager Suite (Jasco).

#### Ceria nanoparticle concentration measured by Inductively coupled plasma atomic emission spectroscopy (ICP-AES)

Twenty microliters of ceria nanoparticle solution were added to 1 mL HNO<sub>3</sub> and 0.5 mL H<sub>2</sub>O<sub>2</sub> (30% wt). Then the samples were transferred into Teflon digestion vials. The vials were placed into an ultraWAVE Single Reaction Chamber (SRC) Microwave Digestor (Milestone), and the reaction chamber was filled with Ar (40 bar). Samples were treated by microwave, and the temperature in the chamber was increased to 240 °C in 20 min and was kept for 10 min, then the chamber cooled down to room temperature in 20 min. Ceria nanoparticles dissolved during the microwave digestion process. The final dissolved solution was diluted to 10 mL, and the cerium element concentration was measured by iCAP 7400 ICP-OES Analyzer (Thermo Scientific) comparing to calibration curve made by cerium standard (1000 mg  $L^{-1}$  Ce in HNO<sub>3</sub>, Sigma-Aldrich). The original ceria solution concentration was calculated by multiplying the dilution factor.

#### Author contributions

V. C. directed the project and oversaw the work. V. C. and Y. H. conceived of the experiments; Y. H. and V. L. performed the experiments; Q. Z. and D. G. contributed to the polymer synthesis; V. L. and Y. B. contributed to antioxidant measurement; C. M. M. and J. D. contributed to phase transfer; Z. X. contributed to TEM images; X. G. and J. V. contributed to DLS and optical absorption measurements. V. C. and Y. H. analyzed all results and made figures. V. C. and Y. H. wrote the manuscript. All authors discussed the results and commented on the manuscript.

#### Conflicts of interest

There are no conflicts to declare.

## Acknowledgements

VC acknowledges support of this work from NIH (R01-EY030569), EPA (DV-84001801-0), and NSF (ENG-21356876). We also acknowledge Tony McCormick for guidance and support with image acquisition, Zachary Salena for guidance and support with thermogravimetric analysis, and Elaina Atherton for insights into the relevance and methods of applying antioxidant assays.

#### References

- 1 J. Biener, A. Wittstock, T. Baumann, J. Weissmüller, M. Bäumer and A. Hamza, Surface chemistry in nanoscale materials, Materials, 2009, 2(4), 2404-2428.
- 2 C. Xu and X. Qu, Cerium oxide nanoparticle: A remarkably versatile rare earth nanomaterial for biological applications, NPG Asia Mater., 2014, 6(3), e90-e90.
- 3 S. Deshpande, S. Patil, S. V. Kuchibhatla and S. Seal, Size dependency variation in lattice parameter and valency states in nanocrystalline cerium oxide, Appl. Phys. Lett., 2005, 87(13), 133113.
- 4 A. Asati, S. Santra, C. Kaittanis, S. Nath and J. M. Perez, Oxidase-like activity of polymer-coated cerium oxide nanoparticles, Angew. Chem., Int. Ed., 2009, 48(13), 2308-2312.
- 5 S. S. Lee, W. Song, M. Cho, H. L. Puppala, N. Phuc, H. Zhu, L. Segatori and V. L. Colvin, Antioxidant properties of cerium oxide nanocrystals as a function of nanocrystal diameter and surface coating, ACS Nano, 2013, 7(11), 9693-9703.
- 6 B. Nelson, M. Johnson, M. Walker, K. Riley and C. Sims, Antioxidant cerium oxide nanoparticles in biology and medicine, Antioxidants, 2016, 5(2), 15.
- 7 C. Korsvik, S. Patil, S. Seal and W. T. Self, Superoxide dismutase mimetic properties exhibited by vacancy engineered ceria nanoparticles, Chem. Commun., 2007, (10), 1056.
- 8 S. M. Hirst, A. S. Karakoti, R. D. Tyler, N. Sriranganathan, S. Seal and C. M. Reilly, Anti-inflammatory properties of cerium oxide nanoparticles, Small, 2009, 5(24), 2848-2856.
- 9 L. L. Wong, S. M. Hirst, Q. N. Pye, C. M. Reilly, S. Seal and J. F. McGinnis, Catalytic nanoceria are preferentially retained in the rat retina and are not cytotoxic after intravitreal injection, *PLoS One*, 2013, **8**(3), e58431.
- 10 A. Pinna, L. Malfatti, G. Galleri, R. Manetti, S. Cossu, G. Rocchitta, R. Migheli, P. A. Serra and P. Innocenzi, Ceria nanoparticles for the treatment of Parkinson-like diseases induced by chronic manganese intoxication, RSC Adv., 2015, 5(26), 20432-20439.
- 11 H. J. Kwon, M.-Y. Cha, D. Kim, D. K. Kim, M. Soh, K. Shin, T. Hyeon and I. Mook-Jung, Mitochondria-targeting ceria nanoparticles as antioxidants for Alzheimer's disease, ACS Nano, 2016, 10(2), 2860-2870.
- 12 E. Atherton, Y. Hu, S. Brown, E. Papiez, V. Ling, V. L. Colvin and D. A. Borton, A 3D in vitro model of the device-tissue interface: Functional and structural symptoms of innate neuroinflammation are mitigated by antioxidant ceria nanoparticles, J. Neural Eng., 2022, 19(3), 036004.
- 13 I. Celardo, M. De Nicola, C. Mandoli, J. Z. Pedersen, E. Traversa and L. Ghibelli, Ce<sup>3+</sup> ions determine redoxdependent anti-apoptotic effect of cerium oxide nanoparticles, ACS Nano, 2011, 5(6), 4537-4549.
- 14 L. Chen, P. Fleming, V. Morris, J. D. Holmes and M. A. Morris, Size-related lattice parameter changes and surface defects in ceria nanocrystals, J. Phys. Chem. C, 2010, 114(30), 12909-12919.

- 15 S. A. Acharya, V. M. Gaikwad, V. Sathe and S. K. Kulkarni, Influence of gadolinium doping on the structure and defects of ceria under fuel cell operating temperature, Appl. Phys. Lett., 2014, 104(11), 113508.
- 16 H.-X. Mai, L.-D. Sun, Y.-W. Zhang, R. Si, W. Feng, H.-P. Zhang, H.-C. Liu and C.-H. Yan, Shape-selective synthesis and oxygen storage behavior of ceria nanopolyhedra, nanorods, and nanocubes, *J. Phys. Chem. B*, 2005, **109**(51), 24380-24385.
- 17 S. Tsunekawa, R. Sivamohan, S. Ito, A. Kasuya and T. Fukuda, Structural study on monosize CeO<sub>2-x</sub> nanoparticles, Nanostruct. Mater., 1999, 11(1), 141-147.
- 18 K. Rahme, L. Chen, R. G. Hobbs, M. A. Morris, C. O'Driscoll and J. D. Holmes, PEGylated gold nanoparticles: Polymer quantification as a function of PEG lengths and nanoparticle dimensions, RSC Adv., 2013, 3(17), 6085-6094.
- 19 L. X. Chen, T. Liu, M. C. Thurnauer, R. Csencsits and T. Rajh, Fe<sub>2</sub>O<sub>3</sub> Nanoparticle structures investigated by x-ray absorption near-edge structure, surface modifications, and model calculations. The, J. Phys. Chem. B, 2002, 106(34), 8539-8546.
- 20 U. El-Ayaan, E. Herlinger, R. F. Jameson and W. Linert, Anaerobic oxidation of dopamine by iron(III), J. Chem. Soc., Dalton Trans., 1997, 16, 2813-2818.
- 21 M. D. Shultz, J. U. Reveles, S. N. Khanna and E. E. Carpenter, Reactive nature of dopamine as a surface functionalization agent in iron oxide nanoparticles, J. Am. Chem. Soc., 2007, **129**(9), 2482-2487.
- 22 A. K. L. Yuen, G. A. Hutton, A. F. Masters and T. Maschmeyer, The interplay of catechol ligands with nanoparticulate iron oxides, Dalton Trans., 2012, 41(9), 2545.
- 23 E. Sharpe, T. Frasco, D. Andreescu and S. Andreescu, Portable ceria nanoparticle-based assay for rapid detection of foodantioxidants (NanoCerac), Analyst, 2013, 138(1), 249-262.
- 24 R. E. Ozel, A. Hayat, K. N. Wallace and S. Andreescu, Effect of cerium oxide nanoparticles on intestinal serotonin in zebrafish, RSC Adv., 2013, 3(35), 15298-15309.
- 25 D. Andreescu, G. Bulbul, R. E. Özel, A. Hayat, N. Sardesai and S. Andreescu, Applications and implications of nanoceria reactivity: Measurement tools and environmental impact, Environ. Sci.: Nano, 2014, 1(5), 445-458.
- 26 G. Bülbül, A. Hayat, X. Liu and S. Andreescu, Reactivity of nanoceria particles exposed to biologically relevant catechol-containing molecules, RSC Adv., 2016, 6(65), 60007-60014.
- 27 A. Lassenberger, O. Bixner, T. Gruenewald, H. Lichtenegger, R. Zirbs and E. Reimhult, Evaluation of high-yield purification methods on monodisperse peg-grafted iron oxide nanoparticles, Langmuir, 2016, 32(17), 4259-4269.
- 28 S. S. Lee, H. Zhu, E. Q. Contreras, A. Prakash, H. L. Puppala and V. L. Colvin, High temperature decomposition of cerium precursors to form ceria nanocrystal libraries for biological applications, Chem. Mater., 2012, 24(3), 424-432.
- 29 D. R. Mullins, The surface chemistry of cerium oxide, Surf. Sci. Rep., 2015, 70(1), 42-85.

- 30 M. Kurian and C. Kunjachan, Investigation of size dependency on lattice strain of nanoceria particles synthesised by wet chemical methods, Int. Nano Lett., 2014, 4(4), 73-80.
- 31 J. Borges, J. A. Ribeiro, E. M. Pereira, C. A. Carreira, C. M. Pereira and F. Silva, Preparation and characterization of DNA films using olevlamine modified Au surfaces, J. Colloid Interface Sci., 2011, 358(2), 626-634.
- 32 C. K. Kim, T. Kim, I.-Y. Choi, M. Soh, D. Kim, Y.-J. Kim, H. Jang, H.-S. Yang, J. Y. Kim, H.-K. Park, S. P. Park, S. Park, T. Yu, B.-W. Yoon, S.-H. Lee and T. Hyeon, Ceria nanoparticles that can protect against ischemic stroke, Angew. Chem., Int. Ed., 2012, 51(44), 11039-11043.
- 33 E. Amstad, T. Gillich, I. Bilecka, M. Textor and E. Reimhult, Ultrastable iron oxide nanoparticle colloidal suspensions using dispersants with catechol-derived anchor groups, Nano Lett., 2009, 9(12), 4042-4048.
- 34 A. El-Faham, R. S. Funosas, R. Prohens and F. Albericio, COMU: A safer and more effective replacement for benzotriazole-based uronium coupling reagents, Chem. - Eur. J., 2009, 15(37), 9404-9416.
- 35 J. M. Dust, Z. H. Fang and J. M. Harris, Proton NMR characterization of poly(ethylene glycols) and derivatives, Macromolecules, 1990, 23(16), 3742-3746.
- 36 A. Alalaiwe, G. Roberts, P. Carpinone, J. Munson and S. Roberts, Influence of PEG coating on the oral bioavailability of gold nanoparticles in rats, Drug Delivery, 2017, 24(1), 591-598.
- 37 D. N. Benoit, H. Zhu, M. H. Lilierose, R. A. Verm, N. Ali, A. N. Morrison, J. D. Fortner, C. Avendano and V. L. Colvin, Measuring the grafting density of nanoparticles in solution by analytical ultracentrifugation and total organic carbon analysis, Anal. Chem., 2012, 84(21), 9238-9245.
- 38 M. Uz, V. Bulmus and S. Alsoy Altinkaya, Effect of peg grafting density and hydrodynamic volume on gold nanoparticle-cell interactions: An investigation on cell cycle, apoptosis, and DNA damage, Langmuir, 2016, 32(23), 5997-6009.
- 39 P. Kingshott, H. Thissen and H. J. Griesser, Effects of cloudpoint grafting, chain length, and density of PEG layers on competitive adsorption of ocular proteins, Biomaterials, 2002, 23(9), 2043-2056.
- 40 C. Chevigny, D. Gigmes, D. Bertin, J. Jestin and F. Boué, Polystyrene grafting from silica nanoparticles via nitroxidemediated polymerization (NMP): Synthesis and SANS analysis with the contrast variation method, Soft Matter, 2009, 5(19), 3741.
- 41 J. Balla, T. Kiss and R. F. Jameson, Copper(II)-catalyzed oxidation of catechol by molecular oxygen in aqueous solution, Inorg. Chem., 1992, 31(1), 58-62.
- 42 E. L. Cavalieri, K.-M. Li, N. Balu, M. Saeed, P. Devanesan, S. Higginbotham, J. Zhao, M. L. Gross and E. G. Rogan, Catechol *ortho*-quinones: The electrophilic compounds that

- form depurinating DNA adducts and could initiate cancer and other diseases, Carcinogenesis, 2002, 23(6), 1071-1077.
- 43 B. Fang, A study of the Ce(III)/Ce(IV) redox couple for redox flow battery application, Electrochim. Acta, 2002, 47(24), 3971-3976.
- 44 D. O. Whittemore and D. Langmuir, Standard electrode potential of  $Fe^{3+} + e^{-} = Fe^{2+}$  from 5-35.deg, J. Chem. Eng. Data, 1972, 17(3), 288-290.
- 45 N. Holten-Andersen, M. J. Harrington, H. Birkedal, B. P. Lee, P. B. Messersmith, K. Y. C. Lee and J. H. Waite, pH-induced metal-ligand cross-links inspired by mussel yield selfhealing polymer networks with near-covalent elastic moduli, Proc. Natl. Acad. Sci. U. S. A., 2011, 108(7), 2651-2655.
- 46 A. Hayat, J. Cunningham, G. Bulbul and S. Andreescu, Evaluation of the oxidase like activity of nanoceria and its application in colorimetric assays, Anal. Chim. Acta, 2015, 885, 140-147.
- 47 W. J. Barreto, S. Ponzoni and P. Sassi, A Raman and UV-Vis study of catecholamines oxidized with Mn(III), Spectrochim. Acta, Part A, 1998, 55(1), 65-72.
- 48 A. Hayat, D. Andreescu, G. Bulbul and S. Andreescu, Redox reactivity of cerium oxide nanoparticles against dopamine, J. Colloid Interface Sci., 2014, 418, 240-245.
- 49 F. Zhang, P. Wang, J. Koberstein, S. Khalid and S.-W. Chan, Cerium oxidation state in ceria nanoparticles studied with X-ray photoelectron spectroscopy and absorption near edge spectroscopy, Surf. Sci., 2004, 563(1), 74-82.
- 50 B. Choudhury, P. Chetri and A. Choudhury, Oxygen defects and formation of Ce3+ affecting the photocatalytic performance of CeO<sub>2</sub> nanoparticles, RSC Adv., 2014, 4(9), 4663-4671.
- 51 A. Marino, C. Tonda-Turo, D. De Pasquale, F. Ruini, G. Genchi, S. Nitti, V. Cappello, M. Gemmi, V. Mattoli, G. Ciardelli and G. Ciofani, Gelatin/nanoceria nanocomposite fibers as antioxidant scaffolds for neuronal regeneration, Biochim. Biophys. Acta, Gen. Subj., 2017, 1861(2), 386-395.
- 52 Z. Tian, X. Li, Y. Ma, T. Chen, D. Xu, B. Wang, Y. Qu and Y. Gao, Quantitatively intrinsic biomimetic catalytic activity of nanocerias as radical scavengers and their ability against H<sub>2</sub>O<sub>2</sub> and doxorubicin-induced oxidative stress, ACS Appl. Mater. Interfaces, 2017, 9(28), 23342-23352.
- 53 B. J. R. Gregório, I. I. Ramos, L. M. Magalhães, E. M. P. Silva, S. Reis and M. A. Segundo, Microplate ORAC-pyranine spectrophotometric assay for high-throughput assessment of antioxidant capacity, Microchem. J., 2020, 158, 105156.
- 54 B. Ou, M. Hampsch-Woodill and R. L. Prior, Development and validation of an improved oxygen radical absorbance capacity assay using fluorescein as the fluorescent probe, J. Agric. Food Chem., 2001, 49(10), 4619-4626.
- 55 A. L. Patterson, The Scherrer formula for X-ray particle size determination, Phys. Rev., 1939, 56(10), 978-982.